

**Supramolecular Chemistry**

How to cite:

International Edition: doi.org/10.1002/anie.202107903

German Edition: doi.org/10.1002/ange.202107903

# Chemoresponsive Supramolecular Polypseudorotaxanes with Infinite Switching Capability

 Yitao Wu, Liqing Shangguan, Qi Li, Jiajun Cao, Yang Liu, Zeju Wang, Huangtianzhi Zhu,\*  
Feng Wang,\* and Feihe Huang\*

**Abstract:** Chemoresponsive supramolecular systems with infinite switching capability are important for applications in recycled materials and intelligent devices. To attain this objective, here a chemoresponsive polypseudorotaxane is reported on the basis of a bis(*p*-phenylene)-34-crown-10 macrocycle (**H**) and a cyano-substituted viologen guest (**G**). **H** and **G** form a [2]pseudorotaxane (**H**⊃**G**) both in solution and in the solid state. Upon addition of AgSF<sub>6</sub>, a polypseudorotaxane (denoted as [**H**·**G**·Ag]<sub>n</sub>) forms as synergistically driven by host–guest complexation and metal-coordination interactions. [**H**·**G**·Ag]<sub>n</sub> depolymerizes into a [3]pseudorotaxane (denoted as **H**<sub>2</sub>·**G**·Ag<sub>2</sub>·acetone<sub>2</sub>) upon addition of **H** and AgSF<sub>6</sub>, while it reforms with successive addition of **G**. The transformations between [**H**·**G**·Ag]<sub>n</sub> and **H**<sub>2</sub>·**G**·Ag<sub>2</sub>·acetone<sub>2</sub> can be switched for infinite cycles, superior to the conventional chemoresponsive supramolecular polymeric systems with limited switching capability.

## Introduction

Chemical triggers are important to modify the structures and functions of biological systems, as illustrated by the denaturation and renaturation processes encountered in lipid bilayers, proteins, and DNA.<sup>[1]</sup> Inspired by these fascinating behaviors, chemists have devoted great efforts to construct

artificial chemoresponsive systems.<sup>[2]</sup> Supramolecular polymers, as pioneered by Lehn and Meijer, denote the polymeric arrays of monomer units held together by reversible non-covalent interactions.<sup>[3]</sup> When chemical triggers weaken or destroy the noncovalent bonds in supramolecular polymers, stimuli-responsiveness can be amplified from the molecular to the macroscopic level, which is intriguing for the fabrication of adaptive materials.<sup>[4]</sup> Despite the progress achieved in this field, the invasive character of chemical triggers produces wastes and thereby changes the original environment, hampering structural reformation of supramolecular polymers.<sup>[5]</sup> Therefore, for state-of-art chemoresponsive supramolecular polymers, their reversibility can be operated for limited cycles, detrimental for the applications in recycled materials and intelligent devices.<sup>[6]</sup> It remains challenging to develop supramolecular polymers with infinite chemo-switching capability.

Since the accidental discovery of dibenzo[18]crown-6 by Pedersen in 1967,<sup>[7]</sup> synthetic macrocycles such as crown ethers, cyclodextrins, calixarenes, pillararenes, and cucurbiturils have attracted tremendous attention due to their highly specific and selective complexation toward the complementary guests.<sup>[8–12]</sup> Macrocycle-directed supramolecular polymerization was achieved by Gibson,<sup>[13]</sup> Harada,<sup>[14]</sup> and our group,<sup>[15]</sup> by employing macrocyclic receptor/guest recognition as the non-covalent connecting units. Additionally, Zhang's and Stoddart's groups threaded the macrocycles onto the linker units.<sup>[16,17]</sup> It rigidified supramolecular monomers, facilitating linear supramolecular polymerization rather than cyclic oligomerization. We envisage that the elaborate combination of the above two roles of macrocycles will be able to pave the way for chemo-reversible supramolecular polymerization/depolymerization with infinite switching capability. On one hand, the presence of excess macrocycles gives rise to supramolecular depolymerization via the “chain-stopping” effect. On the other hand, these macrocycles can move back to the linking point of supramolecular monomers, leading to supramolecular repolymerization under the specific chemical triggering conditions. By taking advantage of the adaptive macrocycle/guest complexation character, we can solve the irreversible issues encountered in traditional chemoresponsive supramolecular polymeric systems.

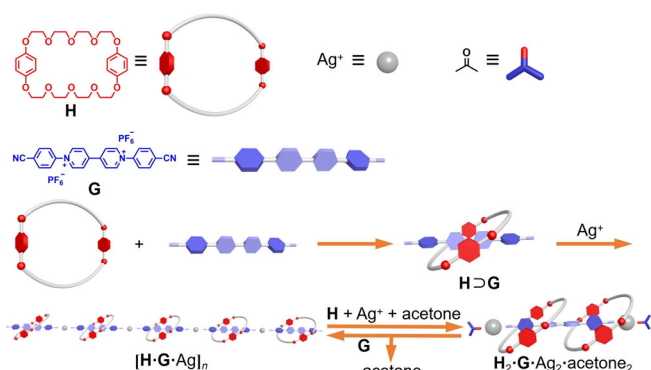
To attain this objective, herein a novel supramolecular polymer (denoted as [**H**·**G**·Ag]<sub>n</sub>, Scheme 1), namely a polypseudorotaxane, has been developed. At first, a [2]pseudorotaxane (**H**⊃**G**) was fabricated from a bis(*p*-phenylene)-34-crown-10 (**H**) macrocycle and a paraquat guest (**G**) with the presence of two cyano groups. It self-assembled into

[\*] Y. Wu, Dr. L. Shangguan, Q. Li, J. Cao, Y. Liu, Z. Wang, H. Zhu, Prof. Dr. F. Huang  
State Key Laboratory of Chemical Engineering  
Key Laboratory of Excited-State Materials of Zhejiang Province  
Stoddart Institute of Molecular Science, Department of Chemistry  
Zhejiang University, Hangzhou 310027 (P. R. China)  
E-mail: htzzhu@zju.edu.cn  
fhuang@zju.edu.cn

Prof. Dr. F. Wang  
CAS Key Laboratory of Soft Matter Chemistry  
Department of Polymer Science and Engineering  
University of Science and Technology of China  
Hefei 230026 (P. R. China)  
E-mail: drfwang@ustc.edu.cn

Prof. Dr. F. Huang  
ZJU-Hangzhou Global Scientific and  
Technological Innovation Center  
Hangzhou 311215 (P. R. China)  
and  
Green Catalysis Center and College of Chemistry  
Zhengzhou University, Zhengzhou 450001 (P. R. China)

 Supporting information and the ORCID identification number(s) for the author(s) of this article can be found under:  
<https://doi.org/10.1002/anie.202107903>.



**Scheme 1.** Chemical structures and representations of **H**, **G**,  $\text{Ag}^+$  and acetone, and representations of the formation of [2]pseudorotaxane  $\text{H}\supset\text{G}$  from **H** and **G**, together with the reversible transformations between polypseudorotaxane  $[\text{H}\cdot\text{G}\cdot\text{Ag}]_n$  and [3]pseudorotaxane  $\text{H}_2\cdot\text{G}\cdot\text{Ag}_2\cdot\text{acetone}_2$ .

$[\text{H}\cdot\text{G}\cdot\text{Ag}]_n$  upon metal–ligand coordination between the cyano groups and  $\text{Ag}^+$  cation. Upon adding an excess of **H** and  $\text{Ag}^+$  cation in acetone,  $[\text{H}\cdot\text{G}\cdot\text{Ag}]_n$  depolymerizes to a [3]pseudorotaxane (denoted as  $\text{H}_2\cdot\text{G}\cdot\text{Ag}_2\cdot\text{acetone}_2$ ) through adaptive host–guest reorganization. The successive addition of **G** removed the “chain-stopping” effect of **H**, giving rise to the revival of  $[\text{H}\cdot\text{G}\cdot\text{Ag}]_n$ . Thanks to the absence of waste formation, the depolymerization/repolymerization processes switched reversibly and adaptively for infinite cycles, which is promising for applications in functional materials with degradable and self-healing properties.

## Results and Discussion

First, host–guest recognition between **H** and **G** was established and characterized. As shown in Figure 1, after mixing equimolar **H** and **G** in  $[\text{D}_6]$ acetone, the proton nuclear magnetic resonance ( $^1\text{H}$  NMR) signals relating to protons  $\text{H}_{1,2}$  of pyridinium rings of **G** exhibited upfield shifts, while protons  $\text{H}_{3,4}$  of phenyl rings of **G** shifted downfield. Meanwhile, the peaks relating to protons  $\text{H}_{a-d}$  on **H** revealed upfield

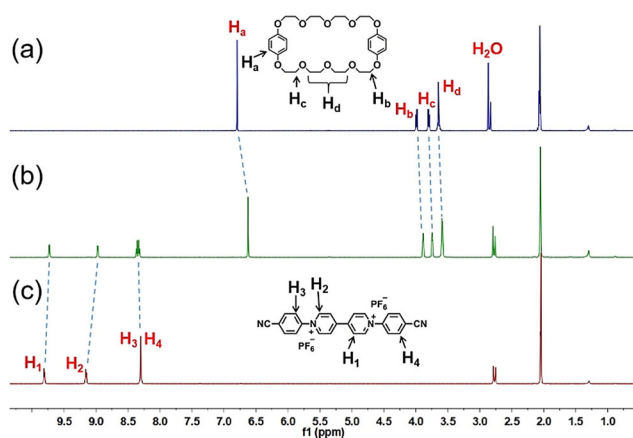


**Figure 1.** Partial  $^1\text{H}$  NMR spectra (600 MHz,  $[\text{D}_6]$ acetone, 298 K): a) 10.0 mM **H**; b) 10.0 mM **H** and **G**; c) 10.0 mM **G**.

shifts. The 2D nuclear Overhauser effect spectroscopy (NOESY) spectrum of  $\text{H}\supset\text{G}$  showed nuclear Overhauser effect (NOE) signals between  $\text{H}_{a-d}$  of **H** and  $\text{H}_{1-4}$  of **G**, proving the host–guest complexation between **H** and **G** (Figure S6). The binding thermodynamics of  $\text{H}\supset\text{G}$  were acquired via  $^1\text{H}$  NMR titration experiments (298 K,  $[\text{D}_6]$ acetone). According to a molar ratio plot (Figure S9), the complexation stoichiometry was 1:1 (Figure S10). The association constant ( $K_a$ ) of  $\text{H}\supset\text{G}$  was determined to be  $(6.10 \pm 0.24) \times 10^2 \text{ M}^{-1}$  by employing a nonlinear curve-fitting method (Figure S11).<sup>[18]</sup>

Yellow single crystals of  $\text{H}\supset\text{G}$  were obtained by slowly evaporating an acetone solution of equimolar **H** and **G**. The host–guest complex crystal structure (Figure 2) was analyzed via single crystal X-ray crystallography. As shown in Figure 2,  $\text{H}\supset\text{G}$  with a 1:1 complexation stoichiometry was observed in the solid state. The complexation was driven by C–H...O interactions between the hydrogen atoms on **G** and the oxygen atoms on **H** with the distances of 2.585 Å (Figures 2 and S3). The phenylene rings of **H** were  $\pi$ -stacked with both pyridinium rings of **G** with the centroid–centroid distances of 3.372 and 4.332 Å (Figures 2 and S3). The dihedral angles between phenylene rings and pyridinium rings were determined to be 7.61° (Figures 2 and S3). Accordingly,  $\text{H}\supset\text{G}$

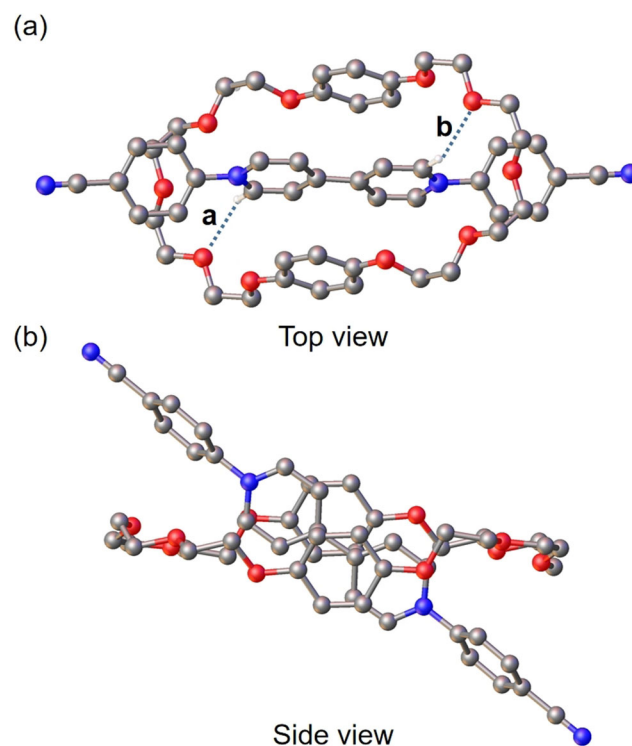


**Figure 2.** The single-crystal structure of  $\text{H}\supset\text{G}$ : a) top view; b) side view. C gray, O red, N blue.  $\text{PF}_6^-$  ions, acetone molecules, and H atoms except the ones involved in hydrogen bonding interactions between **H** and **G** were omitted for clarity. Hydrogen-bond parameters:  $\text{H}\cdots\text{O}$  distances [Å],  $\text{C}\cdots\text{O}$  distances [Å] and  $\text{C}-\text{H}\cdots\text{O}$  angles [deg] of  $\text{C}-\text{H}\cdots\text{O}$  hydrogen bonds: a, 2.585, 3.428, 148.06; b, 2.585, 3.428, 148.06. Face-to-face  $\pi$ -stacking parameters: centroid–centroid distances [Å], 3.732, 3.732, 4.332, 4.332; ring plane/ring plane inclinations [deg], 7.61, 7.61, 7.61, 7.61. The centroid–centroid distance [Å] and dihedral angle [deg] between the two pyridium rings of **G**: 4.288 and 0.<sup>[20]</sup>



displayed a typical [2]pseudorotaxane structure. The cyano groups were located outside of the cavity, rendering it suitable for metal-coordination.

We then sought to fabricate a linear supramolecular polymer, whose formation was driven by metal-coordination interactions with the **H**⊃**G** recognition motif. As the first step, one equivalent  $\text{AgSbF}_6$  was added to **G**. As shown in Figure 3 a and b, the protons related to **G** became narrow,

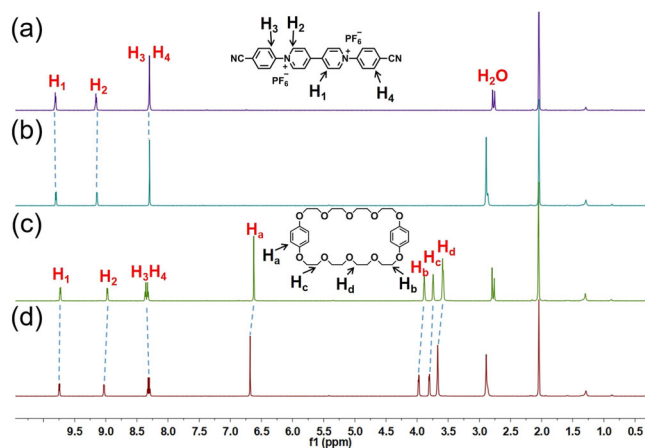


**Figure 3.** Partial  $^1\text{H}$  NMR spectra (600 MHz,  $[\text{D}_6]$ acetone, 298 K): a) 10.0 mM **G**; b) 10.0 mM **G** and  $\text{AgSbF}_6$ ; c) 10.0 mM **H** and **G**; d) 10.0 mM **H**, **G** and  $\text{AgSbF}_6$ .

because of metal-coordination interactions between  $\text{Ag}^+$  and the cyano groups. With reference to the previous reports, it indicated  $\text{Ag}^+$  coordination of **G** into an infinite polymeric chain.<sup>[19]</sup> After validating the fabrication of the linear polymer in the control system, we applied the same procedure in the **H**⊃**G** system toward the fabrication of a polypseudorotaxane. With the addition of one equivalent  $\text{AgSbF}_6$  to a solution of **H**⊃**G**, protons  $\text{H}_{\text{a-d}}$  on **H** revealed downfield shifts due to the decreased electron densities. Protons  $\text{H}_{1,2}$  on **G** revealed downfield shifts and  $\text{H}_{3,4}$  revealed no significant shifts (Figure 3 c and d). These results indicated metal-ligand coordination interactions between **G** and  $\text{Ag}^+$  with no interference from **H**.

Diffusion ordered NMR spectroscopy (DOSY) experiments ( $[\text{D}_6]$ acetone, 298 K) were carried out to prove the formation of a supramolecular polypseudorotaxane at high monomer concentration (Figures S14–S16). Upon addition of equimolar **G** to a solution of **H** (10.0 mM), the signals related to **H** and **G** almost appeared at the same horizontal line in the DOSY spectrum. This suggested the formation of **H**⊃**G**, with a measured diffusion coefficient value of  $8.91 \times 10^{-10} \text{ m}^2 \text{ s}^{-1}$  (Figure S14).  $[\text{H} \cdot \text{G} \cdot \text{Ag}]_n$  was then prepared by adding one equivalent  $\text{AgSbF}_6$  to a solution of **H**⊃**G** (10.0 mM). After addition of  $\text{AgSbF}_6$ , the signals relating to **H**⊃**G** were still located at the same horizontal line in the DOSY spectrum, but with a decreased diffusion coefficient of  $3.89 \times 10^{-10} \text{ m}^2 \text{ s}^{-1}$ . This suggested that the  $\text{Ag}^+$  coordination didn't destroy **H**⊃**G**, while it orthogonally coordinated with the cyano groups to form  $[\text{H} \cdot \text{G} \cdot \text{Ag}]_n$  (Figure S16). Furthermore, the concentration-dependent DOSY experiments revealed

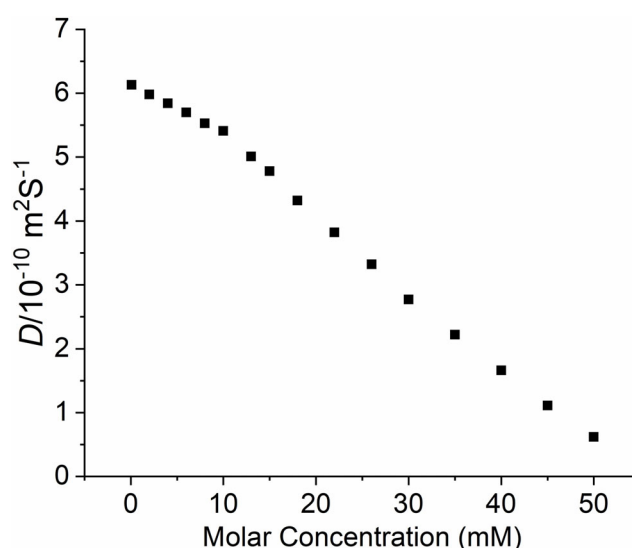


**Figure 4.** Monomer concentration dependence of diffusion coefficient  $D$  (500 MHz,  $[\text{D}_6]$ acetone, 298 K) of  $[\text{H} \cdot \text{G} \cdot \text{Ag}]_n$ .

that as the **H**, **G** and  $\text{AgSbF}_6$  concentrations increased, the diffusion coefficient  $D$  gradually decreased (Figure 4). This result indicated the concentration dependence of the supramolecular polymerization process, giving rise to high molecular weight polypseudorotaxanes at high concentration.

Intriguingly, single crystals of  $[\text{H} \cdot \text{G} \cdot \text{Ag}]_n$  were obtained by slowly evaporating an acetone solution of equimolar **H**, **G** and  $\text{AgSbF}_6$ . As shown in Figure 5 a, the crystal structure exhibited an ordered three-component polypseudorotaxane structure, as synergistically driven by metal-coordination and host–guest interactions (Figures 5 a and S4). In the  $[\text{H} \cdot \text{G} \cdot \text{Ag}]_n$  structure, coordination between the cyano groups and  $\text{Ag}$  atoms formed a linear polymeric structure. The distances of  $\text{Ag} \cdots \text{N}$  coordination bonds were found to be 2.203 and 2.268 Å, with a  $\text{N} \cdots \text{Ag} \cdots \text{N}$  angle of  $135.43^\circ$  (Figure 5 a). Notably, the  $\text{Ag}^+$  cation was also stabilized by three O– $\text{Ag}$  interactions rendered by **H**. Host–guest complexation also existed in the crystal structure, in which **H** was evenly distributed and threaded by the polymer chain. It exhibited C– $\text{H} \cdots \text{O}$  interactions between the hydrogen atoms on **G** and the oxygen atoms on **H**, with distances of 2.225 and 2.639 Å (Figures 5 a and S4). Different from **H**⊃**G**, in the structure of  $[\text{H} \cdot \text{G} \cdot \text{Ag}]_n$ , the phenylene rings of **H** were  $\pi$ -stacked with a phenylene ring of **G**, with a centroid-centroid distance of 4.007 Å (Figure S4). The dihedral angle between the phenylene ring of **H** and the phenylene ring of **G** was determined to be  $6.98^\circ$  (Figure S4). The enhanced donor-acceptor interactions in  $[\text{H} \cdot \text{G} \cdot \text{Ag}]_n$  gave rise to red-colored single crystals, in contrast to the yellow-colored single crystals in case of **H**⊃**G**.

The chemoresponsiveness of  $[\text{H} \cdot \text{G} \cdot \text{Ag}]_n$  was then studied. Considering that **H** provides three cation–oxygen non-covalent bonds toward  $\text{Ag}^+$  in  $[\text{H} \cdot \text{G} \cdot \text{Ag}]_n$  (Figure 5 a), we investigated whether or not **H** could serve as a competitive ligand instead of the cyano units. It behaved like a chain-stopper unit, leading to the breakup of the  $[\text{H} \cdot \text{G} \cdot \text{Ag}]_n$  structure. Interestingly,  $\text{H}_2 \cdot \text{G} \cdot \text{Ag}_2 \cdot \text{acetone}_2$  single crystals were obtained upon adding an excess of **H** and  $\text{AgSbF}_6$  to  $[\text{H} \cdot \text{G} \cdot \text{Ag}]_n$ . The

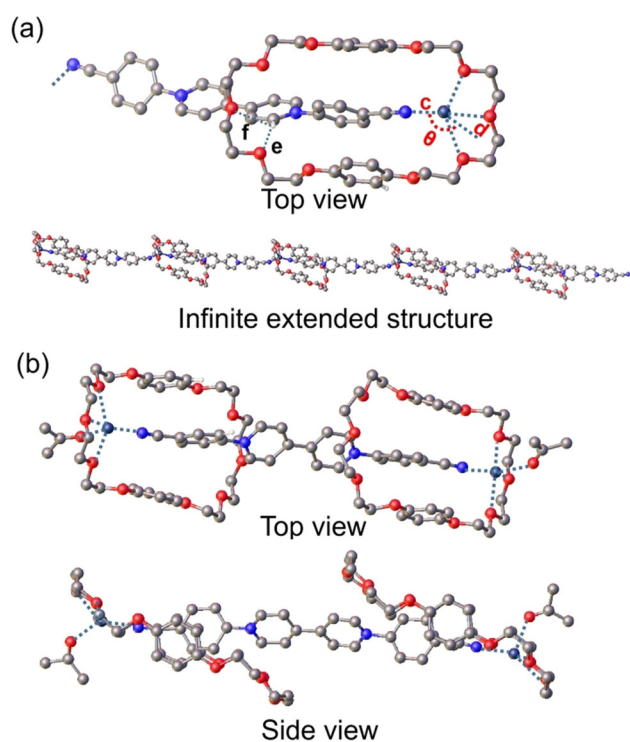


**Figure 5.** Single crystal structures: a)  $[\text{H}\cdot\text{G}\cdot\text{Ag}]_n$ . N $\cdots$ Ag $\cdots$ N bonds parameters:  $c = 2.268 \text{ \AA}$ ;  $d = 2.203 \text{ \AA}$ ;  $\theta = 135.43^\circ$ . b)  $\text{H}_2\cdot\text{G}\cdot\text{Ag}_2\cdot\text{acetone}_2$ . C gray, O red, N light blue, Ag dark blue.  $\text{PF}_6^-$  ions,  $\text{SbF}_6^-$  ions, and H atoms except the ones involved in hydrogen bonding interactions between **H** and **G** were omitted for clarity. Hydrogen-bond parameters: H $\cdots$ O distances [ $\text{\AA}$ ], C $\cdots$ O distances [ $\text{\AA}$ ] and C–H $\cdots$ O angles [deg] of C–H $\cdots$ O hydrogen bonds, e, 2.225, 3.083, 151.290; f, 2.639, 3.078, 108.172. Face-to-face  $\pi$ -stacking parameters: centroid-centroid distances [ $\text{\AA}$ ],  $[\text{H}\cdot\text{G}\cdot\text{Ag}]_n$ , 4.007;  $\text{H}_2\cdot\text{G}\cdot\text{Ag}_2\cdot\text{acetone}_2$ , 3.371, 3.853, 4.071; ring plane/ring plane inclinations (deg),  $[\text{H}\cdot\text{G}\cdot\text{Ag}]_n$ , 6.98;  $\text{H}_2\cdot\text{G}\cdot\text{Ag}_2\cdot\text{acetone}_2$ , 8.43, 14.55, 2.11. The centroid–centroid distance [ $\text{\AA}$ ] and dihedral angle (deg) between the pyridium rings of **G**:  $[\text{H}\cdot\text{G}\cdot\text{Ag}]_n$ , 4.260 and 14.15;  $\text{H}_2\cdot\text{G}\cdot\text{Ag}_2\cdot\text{acetone}_2$ , 4.270 and 6.07.<sup>[20]</sup>

**H**:**G** stoichiometry in  $\text{H}_2\cdot\text{G}\cdot\text{Ag}_2\cdot\text{acetone}_2$  was 2:1 (Figure 5b). Each  $\text{Ag}^+$  cation was coordinated to three oxygen atoms on **H**, one cyano group and one acetone molecule. In the crystal structure, the phenylene rings of **H** were  $\pi$ -stacked with the phenylene rings of **G**, with centroid-centroid distances of 3.371–4.071  $\text{\AA}$  and dihedral angles between phenylene rings of **H** and phenylene rings of **G** of 2.11–14.55° (Figure S5). Hence, upon adding an excess of **H** and  $\text{AgSbF}_6$ ,  $[\text{H}\cdot\text{G}\cdot\text{Ag}]_n$  was destroyed and transformed to  $\text{H}_2\cdot\text{G}\cdot\text{Ag}_2\cdot\text{acetone}_2$ .

According to 2D NOESY spectra, correlation signals existed between  $\text{H}_{a-d}$  of **H** and  $\text{H}_{1-4}$  of **G** in  $[\text{H}\cdot\text{G}\cdot\text{Ag}]_n$ . The results were similar to those of  $\text{H}\supset\text{G}$ , yet different from those of  $\text{H}_2\cdot\text{G}\cdot\text{Ag}_2\cdot\text{acetone}_2$ . The phenomena indicated that the host–guest complexation mode between **H** and **G** was the same in  $[\text{H}\cdot\text{G}\cdot\text{Ag}]_n$  and  $\text{H}\supset\text{G}$ . In comparison,  $\text{H}_2\cdot\text{G}\cdot\text{Ag}_2\cdot\text{acetone}_2$  altered the **H**/**G** complexation structure (Figures S7 and S8). These experimental results matched well with the single-crystal structures of  $\text{H}\supset\text{G}$ ,  $[\text{H}\cdot\text{G}\cdot\text{Ag}]_n$  and  $\text{H}_2\cdot\text{G}\cdot\text{Ag}_2\cdot\text{acetone}_2$  (Figures 2 and 5).

The transformation from  $[\text{H}\cdot\text{G}\cdot\text{Ag}]_n$  to  $\text{H}_2\cdot\text{G}\cdot\text{Ag}_2\cdot\text{acetone}_2$  was also performed in solution. A 10.0 mM  $[\text{H}\cdot\text{G}\cdot\text{Ag}]_n$  solution was prepared at first, followed by the gradual

addition of **H** and  $\text{AgSbF}_6$  as the chain stoppers. DOSY experiments were used to monitor the change of diffusion coefficient  $D$ . As shown in Figure 6a, upon addition of one more equivalent **H** and  $\text{AgSbF}_6$ , the diffusion coefficient of the solution increased, proving the disassembly of  $[\text{H}\cdot\text{G}\cdot\text{Ag}]_n$  to form  $\text{H}_2\cdot\text{G}\cdot\text{Ag}_2\cdot\text{acetone}_2$ . The polymerization of  $\text{H}_2\cdot\text{G}\cdot\text{Ag}_2\cdot\text{acetone}_2$  was reactivated by adding one equivalent of **G**. The diffusion coefficient was decreased along with the addition. The diffusion coefficients of  $[\text{H}\cdot\text{G}\cdot\text{Ag}]_n$  and  $\text{H}_2\cdot\text{G}\cdot\text{Ag}_2\cdot\text{acetone}_2$  were transformed for multiple cycles (Figure 6b). This phenomenon indicated full reversibility between  $[\text{H}\cdot\text{G}\cdot\text{Ag}]_n$  and  $\text{H}_2\cdot\text{G}\cdot\text{Ag}_2\cdot\text{acetone}_2$  with infinite switching capability.

The morphology of  $[\text{H}\cdot\text{G}\cdot\text{Ag}]_n$  was investigated by transmission electron microscopy (TEM) and scanning electron microscopy (SEM). Free **H** and **G** were observed to assemble into random aggregates without a regular morphology, while  $\text{H}_2\cdot\text{G}\cdot\text{Ag}_2\cdot\text{acetone}_2$  self-assembled into spherical structures (Figures S17–S22). By contrast, adding one equivalent of  $\text{AgSbF}_6$  to a solution of **G** or  $\text{H}\supset\text{G}$  led to the appearance of rod-like fibers, suggesting the formation of linear supra-

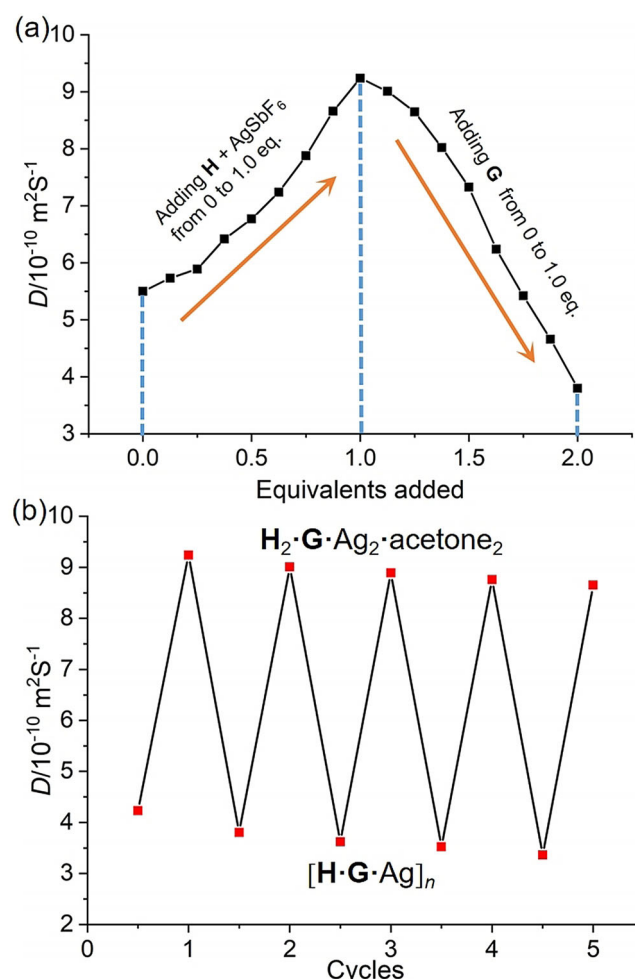


**Figure 6.** Diffusion coefficients  $D$  (500 MHz,  $[\text{D}_6]$ acetone, 298 K) of a)  $[\text{H}\cdot\text{G}\cdot\text{Ag}]_n$  (10.0 mM) upon adding extra **H** +  $\text{AgSbF}_6$  (from 0 to 1.0 equiv.) and **G** (from 0 to 1.0 equiv.) gradually and b) multiple switchings between  $[\text{H}\cdot\text{G}\cdot\text{Ag}]_n$  and  $\text{H}_2\cdot\text{G}\cdot\text{Ag}_2\cdot\text{acetone}_2$ .



molecular polymers via metal-coordination (Figure 7). The morphological conversions between linear structures (derived from  $[\mathbf{H}\cdot\mathbf{G}\cdot\mathbf{Ag}]_n$ ) and spherical structures (derived from  $\mathbf{H}_2\cdot\mathbf{G}\cdot\mathbf{Ag}_2\cdot\text{acetone}_2$ ) were observed for five cycles without waste production (Figure S23).

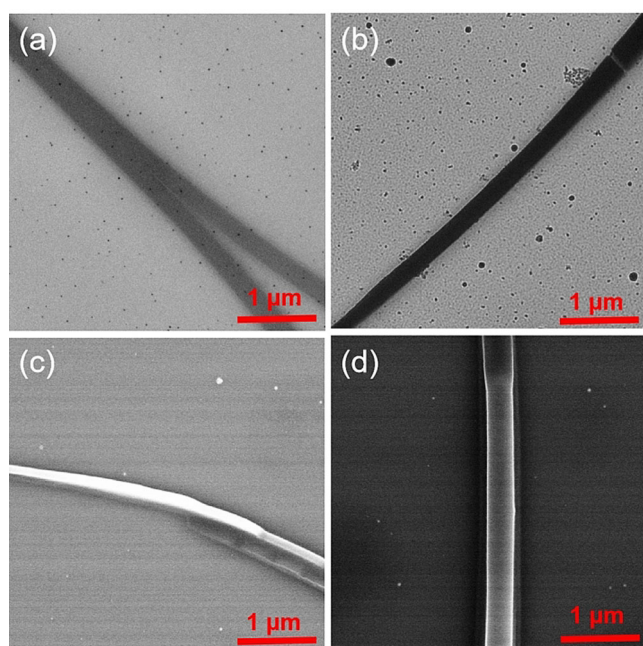


**Figure 7.** TEM images: a)  $[\mathbf{G}\cdot\mathbf{Ag}]_n$ ; b)  $[\mathbf{H}\cdot\mathbf{G}\cdot\mathbf{Ag}]_n$ . SEM images: c)  $[\mathbf{G}\cdot\mathbf{Ag}]_n$ ; d)  $[\mathbf{H}\cdot\mathbf{G}\cdot\mathbf{Ag}]_n$ . Samples were prepared from highly concentrated solutions.

A competitive experiment was performed to show the advantages of such reversible and waste-free chemoresponsive  $[\mathbf{H}\cdot\mathbf{G}\cdot\mathbf{Ag}]_n$  aided by the crown ether macrocycle. Specifically, tetrabutylammonium iodine (TBAI) was employed as a chemical stimulus instead of  $\mathbf{H}$  to break up  $[\mathbf{H}\cdot\mathbf{G}\cdot\mathbf{Ag}]_n$ . As shown in Figure 8, the diffusion coefficient  $D$  of  $[\mathbf{H}\cdot\mathbf{G}\cdot\mathbf{Ag}]_n$  increased from  $3.80 \times 10^{-10} \text{ m}^2 \text{ s}^{-1}$  to  $9.33 \times 10^{-10} \text{ m}^2 \text{ s}^{-1}$  upon adding one equivalent TBAI, while it decreased to  $4.07 \times 10^{-10} \text{ m}^2 \text{ s}^{-1}$  with the further addition of  $\text{AgSbF}_6$ . These results revealed iodide-induced supramolecular depolymerization and  $\text{Ag}^+$ -induced repolymerization (Figures S24–S26). Nevertheless, the depolymerization process was accompanied by the precipitation of  $\text{AgI}$ . Accordingly, the introduction of invasive stimulus TBAI produced chemical waste, which is disadvantageous for multiple-cycle supramolecular polymerization/depolymerization transformations. The results validated the crucial role of  $\mathbf{H}$  for the chemoresponsive supramolecular polymerization with infinite switching cycles.

## Conclusion

A novel supramolecular polypseudorotaxane  $[\mathbf{H}\cdot\mathbf{G}\cdot\mathbf{Ag}]_n$  was constructed with infinite chemo-switching capability. A [2]pseudorotaxane  $\mathbf{H}\cdot\mathbf{G}$  was first prepared based on  $\mathbf{H}$  and  $\mathbf{G}$ . The crystal structure of  $\mathbf{H}\cdot\mathbf{G}$  revealed that the two cyano end groups of  $\mathbf{G}$  were located outside the cavity of  $\mathbf{H}$ , making

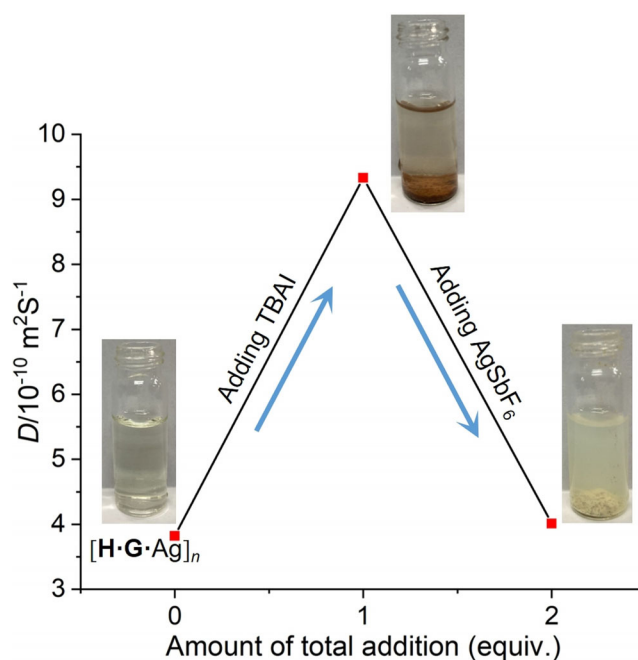


**Figure 8.** Diffusion coefficients  $D$  (500 MHz,  $[\text{D}_6]\text{acetone}$ , 298 K) of  $[\mathbf{H}\cdot\mathbf{G}\cdot\mathbf{Ag}]_n$  (10.0 mM) upon adding one equivalent TBAI and then adding one equivalent  $\text{AgSbF}_6$ .

it suitable for metal-coordination.  $[\mathbf{H}\cdot\mathbf{G}\cdot\mathbf{Ag}]_n$  was prepared by adding one equivalent  $\text{AgSbF}_6$  to a solution of  $\mathbf{H}\cdot\mathbf{G}$ .  $[\mathbf{H}\cdot\mathbf{G}\cdot\mathbf{Ag}]_n$  was dissociated to a [3]pseudorotaxane  $\mathbf{H}_2\cdot\mathbf{G}\cdot\mathbf{Ag}_2\cdot\text{acetone}_2$  upon addition of one more equivalent  $\mathbf{H}$  and  $\text{AgSbF}_6$ , and converted back to the initial state after the successive addition of  $\mathbf{G}$ . The crystal structures and binding modes of  $[\mathbf{H}\cdot\mathbf{G}\cdot\mathbf{Ag}]_n$  and  $\mathbf{H}_2\cdot\mathbf{G}\cdot\mathbf{Ag}_2\cdot\text{acetone}_2$  were confirmed by X-ray crystallographic analysis. In combination with the rod-like and the spherical morphologies observed by TEM and SEM, the inter-conversion between  $[\mathbf{H}\cdot\mathbf{G}\cdot\mathbf{Ag}]_n$  and  $\mathbf{H}_2\cdot\mathbf{G}\cdot\mathbf{Ag}_2\cdot\text{acetone}_2$  can be operated for infinite cycles. Our work demonstrated the controlled formation, dissociation and reformation of a polypseudorotaxane  $[\mathbf{H}\cdot\mathbf{G}\cdot\mathbf{Ag}]_n$  that expands the possibilities for the development of precision engineering of supramolecular polymers.

## Acknowledgements

This work was supported by the National Natural Science Foundation of China (22035006, and 21922110) and the Fundamental Research Funds for the Central Universities (WK3450000005).

## Conflict of Interest

The authors declare no conflict of interest.

**Keywords:** chemoresponsiveness · host–guest systems · polypseudorotaxanes · supramolecular chemistry · supramolecular polymers



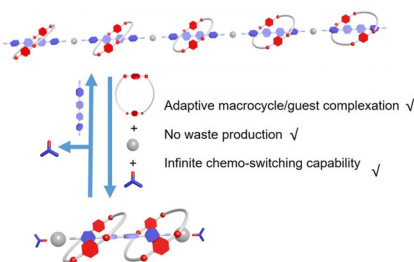
## Research Articles



## Supramolecular Chemistry

Y. Wu, L. Shangguan, Q. Li, J. Cao, Y. Liu,  
Z. Wang, H. Zhu,\* F. Wang,\*  
F. Huang\* ————— ■■■■-■■■■

Chemoresponsive Supramolecular  
Polypseudorotaxanes with Infinite  
Switching Capability



We report a novel polypseudorotaxane  $[\text{H}\cdot\text{G}\cdot\text{Ag}]_n$ , as synergistically driven by host-guest complexation and metal-coordination interactions. It depolymerizes into a [3]pseudorotaxane  $\text{H}_2\cdot\text{G}\cdot\text{Ag}_2\cdot\text{acetone}_2$  upon addition of **H** and  $\text{AgSF}_6$ , while it reforms with successive addition of **G**. The transformations between  $[\text{H}\cdot\text{G}\cdot\text{Ag}]_n$  and  $\text{H}_2\cdot\text{G}\cdot\text{Ag}_2\cdot\text{acetone}_2$  can be switched for infinite cycles.

